J. Appl. Comput. Mech., 6(2) (2020) 296-306
DOI: 10.22055/JACM.2019.29024.1543

ISSN: 2383-4536
jacm.scu.ac.ir

M&MoCS

Shahid Chamran University of Ahvaz

Journal of Applied and Computational Mechanics

Research Paper

Slip Effects on Ohmic Dissipative Non-Newtonian Fluid Flow in the Presence of Aligned Magnetic Field

P. Renuka[1], B. Ganga[2], R. Kalaivanan[3], A.K. Abdul Hakeem[4]

[1] Department of Mathematics, Erode Sengunthar Engineering College, Erode - 638 057, India
[2] Department of Mathematics, Providence College for Women, Coonoor - 643 104, India
[3] Department of Mathematics, Vivekananda College, Madurai - 625 234, India
[4] Department of Mathematics, SRMV College of Arts and Science, Coimbatore - 641 020, India

Received March 22 2019; Revised May 18 2019; Accepted for publication May 21 2019.
Corresponding author: A.K. Abdul Hakeem (abdulhakeem6@gmail.com)

Abstract. The present paper deals with the effects of Ohmic dissipative Casson fluid flow over a stretching sheet in the presence of aligned magnetic field. The present phenomenon also includes the interaction of thermal radiation and velocity slip. The governing boundary layer equations are transformed into a set of ordinary differential equations using the similarity transformations. The dimensionless velocity and temperature profiles are solved analytically using hypergeometric function and numerically by using fourth order Runge-Kutta method with shooting technique. It is noted that the increasing values of Eckert number increases the temperature profile and decreases the local Nusselt number.

Keywords: Aligned magnetic field; Casson fluid; Slip; Thermal radiation; Ohmic dissipation.

1. Introduction

The heat transfer of non-Newtonian fluid from different types of geometries over a stretching sheet has a lot of essential applications, such as in ceramic engineering, oil recovery and filtration. Picchi et al. [1] analyzed the modeling of core-annular and plug flow of non-Newtonian shear-thinning fluids in pipes and capillary tubes. Picchi et al. [2] investigated the Characteristics of stratified flows of non-Newtonian shear-thinning fluids. Casson fluid model is one of the non-Newtonian fluid models. This model is based on a structure model of the interactive behavior of solid and liquid phases of a two-phase suspension. Casson fluid shows yield stress. This model was first introduced by Casson in 1995. Some examples of Casson fluid are as follows: tomato sauce, honey, jelly, soup, concentrated fruit juices, etc. Human blood can also be treated as Casson fluid. Mahanthesh et al. [3] analyzed the Marangoni convection in two-phase flow of dusty Casson fluid. Sailaja et al. [4] presented finite element analysis of Magnetohydrodynamic (MHD) Casson fluid flow pasted a vertical plate. Kumaran et al. [5] studied magnetohydrodynamics Casson and Maxwell flows over a stretching sheet. Hamid et al. [6] investigated the dual solutions and stability analysis of flow and heat transfer of Casson fluid over a stretching sheet. Ullah et al. [7] investigated the MHD flow of Casson fluid over a nonlinearly stretching sheet. Ibrahim et al. [8] analyzed MHD mixed convection flow of a Casson nanofluid over a nonlinear permeable stretching sheet. Kumaran and Sandeep [9] studied the thermophoresis and Brownian motion effects on MHD Casson and Williamson fluids flow with cross diffusion. Abdul Hakeem et al. [10] explored the Casson fluid over an impermeable stretching sheet with heat transfer and inclined magnetic field. Kalaivanan et al. [11] studied effects of aligned magnetic field on slip flow of Casson fluid over a stretching sheet. Abolbashari et al. [12] analyzed the analytical modeling of entropy generation for Casson nano-fluid flow induced by a stretching surface.

Published online: September 03 2019

MHD is the study of the relations of conducting fluids with electromagnetic phenomena which has significant applications in industrial fields. Hydromagnetic boundary layers are observed in a number of technical systems employing liquid metal and plasma flow transverse of magnetic fields. In these cases, the flow control can be realized by the Lorentz force. Rashidi et al. [13] analyzed the convective MHD flow of third grade non-Newtonian fluid over a stretching sheet. Makinde et al. [14] studied the MHD variable viscosity reacting flow over a convectively heated plate in a porous medium with thermophoresis. Kayalvizhi et al. [15] investigated the velocity slip effects on heat and mass fluxes of MHD viscous-Ohmic dissipative flow over a stretching sheet with thermal radiation. Effect of thermal radiation on MHD nanofluid flow and heat transfer by means of two phase model is analyzed by Sheikholeslami et al. [16]. Ganga et al. [17] observed the MHD flow of Boungiorno model nanofluid over a vertical plate with internal heat generation/absorption. Some recent studies concerning the flow and heat transfer analysis of fluid flow in the presence of MHD field can be found in (Gireesha et al. [18], Sandeep and Sulochana [19], Pal and Mandal [20], Abdul Hakeem et al. [21], Raju et al. [22], Abdul Hakeem et al. [23], Veeresh et al. [24] and Turkyilmazoglu [25]).

A close observation of the literature reveals that, so far no one has considered the Ohmic dissipation effects on Casson fluid flow in the presence of aligned magnetic field. The governing non-linear partial differential equations which represent the momentum and energy are transformed into ordinary differential equations with the help of suitable similarity transformations. The transformed boundary layer equations which represent the flow and temperature are solved analytically by using hypergeometric function and numerically using fourth order Runge-Kutta method with shooting technique.

2. Mathematical Formulation

Consider a steady, laminar, two-dimensional boundary layer flow of an incompressible, Casson fluid over a stretching sheet. Aligned magnetic field of strength B_0 is applied along the y-direction, with acute an angle γ. At $\gamma = 90^o$, this magnetic field acts like transverse magnetic field (because $\sin 90^o = 1$).

The rheological equation of state for an isotropic and incompressible flow of a Casson fluid is Ullah et al. [7]

$$\tau_{ij} = \begin{Bmatrix} 2(\mu_B + p_y / \sqrt{2\pi})e_{ij}, \pi > \pi_c \\ 2(\mu_B + p_y / \sqrt{2\pi_c})e_{ij}, \pi < \pi_c \end{Bmatrix}$$

Here $\pi = e_{ij}$ and e_{ij} are the $(i, j)^{th}$ component of the deformation rate, μ_B is plastic dynamic viscosity of the non-Newtonian fluid, p_y is the yield stress of the fluid, π is the product of the component of deformation rate with itself and π_c is a critical value of this product based on the non-Newtonian model.

The equation governing the problem under consideration is given by (Kumaran et al. [5])

$$u_x + v_y = 0 \tag{1}$$

$$uu_x + vu_y = \vartheta \left(1 + \frac{1}{\beta}\right) u_{yy} - \frac{\sigma B_0^2 u}{\rho} \sin^2 \gamma \tag{2}$$

where ϑ is the kinematic viscosity, u is the velocity component of x- direction, v is the velocity component of y-direction, ρ is the fluid density, β is the Casson fluid parameter ($\beta = \mu_B \sqrt{2\pi_c} / p_y$) and σ is the electrical conductivity. The boundary conditions for the velocity field are

$$u = ax + lu_y, v = v_w \quad \text{at} \quad y = 0, \quad u \to 0 \quad \text{as} \quad y \to \infty \tag{3}$$

We introduce the following similarity transformation

$$u = axf_\eta, \; v = -(a\vartheta)^{1/2} f \quad \text{and} \quad \eta = \left(\frac{a}{\vartheta}\right)^{1/2} y \tag{4}$$

Using Eq.(4), Eq. (1) is trivially satisfied and Eq. (2) and Eq. (3) take the form

$$\left(1 + \frac{1}{\beta}\right) f_{\eta\eta\eta} + f f_{\eta\eta} - f_\eta^2 - Mn f_\eta \sin^2 \gamma = 0 \tag{5}$$

with the corresponding boundary conditions

$$\begin{aligned} f_\eta &= 1 + Lf_{\eta\eta} \quad \text{at} \quad \eta = 0 \\ f_\eta &\to 0 \quad \text{as} \quad \eta \to \infty \end{aligned} \tag{6}$$

The subscript η denotes differentiation with respect to η. Here Mn is the magnetic parameter ($Mn = \sigma B_0^2 / \rho a$) and L is the slip parameter ($L = l\sqrt{a/\vartheta}$). The solution of Eq. (5) subject to boundary conditions Eq. (6) can be found in the form,

$$f(\eta) = X\left(\frac{1-e^{-\alpha\eta}}{\alpha}\right) \tag{7}$$

where $X = (L\alpha+1)^{-1}$, and we have

$$\alpha = -\frac{1+\beta}{3(L+L\beta)} - \frac{\alpha_1}{3(2^{2/3})(L+L\beta)(\alpha_2+\sqrt{(\alpha_2^2+4\alpha_1^3)^{1/3}})} + \frac{\alpha_2+\sqrt{(\alpha_2^2+4\alpha_1^3)^{1/3}}}{6(2^{1/3})(L+L\beta)}$$

$$\alpha_1 = -4(1+\beta)^2 + 6(L+L\beta)(-L\,Mn\,\beta + LMn\beta\cos 2\gamma)$$

$$\alpha_2 = -16-(48-216L^2-72L^2Mn+72L^2Mn\cos 2\gamma)\beta-(48-432L^2-144L^2Mn+144L^2Mn\cos 2\gamma)\beta^2$$
$$-(16-216L^2-72L^2Mn+72L^2Mn\cos 2\gamma)\beta^3$$

Substituting (7) in (4), the velocity components are

$$u = \frac{ax}{L\alpha+1}e^{-\alpha\eta} \qquad \text{and} \qquad v = -\sqrt{a\vartheta}\left(\frac{1-e^{-\alpha\eta}}{\alpha(L\alpha+1)}\right)$$

The wall shearing stress (stretching sheet) is given by

$$\tau_w = \left(\vartheta u_y\right)_{y=0} \tag{8}$$

The local skin-friction coefficient (frictional drag) is written as

$$C_f = \frac{\tau_w}{\rho u_w^{\,2}} = \mathrm{Re}_x^{\,-1/2}\left(1+\frac{1}{\beta}\right)f_{\eta\eta}(0) \tag{9}$$

where $\mathrm{Re}_x = xu_w / \vartheta$ is the Reynolds number.

3. Heat Transfer Analysis

The governing thermal boundary layer equation of incompressible Casson fluid are stated as follows (Mishra et al. [26])

$$uT_x + vT_y = \frac{k}{\rho c_p}T_{yy} - \frac{1}{\rho c_p}(q_r)_y + \frac{\sigma B_0^2 u^2}{\rho c_p}\sin^2\gamma \tag{10}$$

where T is the temperature, k is the thermal conductivity, ρ is the density and c_p is the specific heat of constant pressure. The Rosseland diffusion approximation for radiation heat flux is given by

$$q_r = -\frac{4\sigma^*}{3k^*}T_y^4 \tag{11}$$

where σ^* is the Stefan-Boltzmann constant and k^* is the mean absorption coefficient. Further, we assume that the temperature difference within flow is such that T^4 may be expanded in a Taylor series. Hence expanding T^4 about T_∞ and neglecting higher order terms we get

$$T^4 \cong 4T_\infty^3 T - 3T_\infty^4 \tag{12}$$

Substituting Eq. (11) and Eq. (12) in Eq. (10), we obtain

$$uT_x + vT_y = \frac{k}{\rho c_p}T_{yy} + \left(\frac{1}{3\rho c_p}\right)\left(\frac{16\sigma^* T_\infty^3}{k^*}\right)T_{yy} + \frac{\sigma B_0^2 u^2}{\rho c_p}\sin^2\gamma \tag{13}$$

The solution of Eq. (13) is found using two types of general heating processes such as prescribed surface temperature (PST) and prescribed power law of surface heat flux (PHF) conditions as described below.

3.1 The prescribed surface temperature (PST CASE)

The boundary conditions in the PST case are given by

$$\begin{aligned} T = T_w = T_\infty + A\left(\frac{x}{l}\right)^2 \qquad \text{at} \quad y = 0\,, \\ T \to T_\infty \qquad \text{as} \quad y \to \infty \end{aligned} \tag{14}$$

where l is the characteristic length, T_w is the temperature of the sheet and T_∞ is the temperature of the fluid far away from the sheet. Define the non-dimensional temperature $\theta(\eta)$ as

$$\theta(\eta) = \frac{T - T_\infty}{T_w - T_\infty} \tag{15}$$

Now, we make use of the transformations given by Eq. (4) and Eq. (15) in Eq. (13). This leads to the non-dimensional form of temperature equation as follows:

$$\omega\theta_{\eta\eta} + \Pr f\theta_\eta - 2\Pr f_\eta\theta + Ec\Pr Mn f_\eta^2 \sin^2\gamma = 0 \tag{16}$$

where $\omega = \dfrac{3N+4}{3N}$, $\Pr = \dfrac{\mu c_p}{k}$ is the Prandtl number, $Ec = \dfrac{u_w^2}{c_p\left(T_w - T_\infty\right)}$ is the Eckert number, $N = \dfrac{kk^*}{4\sigma^* T_\infty^3}$ is the radiation parameter. The boundary conditions in Eq. (14) take the form,

$$\begin{aligned} \theta(\eta) = 1 \qquad \text{at} \quad \eta = 0\,, \\ \theta(\eta) \to 0 \qquad \text{as} \quad \eta \to \infty \end{aligned} \tag{17}$$

An analytical solution of Eq. (16), subject to boundary conditions in Eq. (17) can be obtained in terms of confluent hypergeometric function as

$$\theta(\eta) = c_1 e^{-\alpha\left(\frac{a0+bo}{2}\right)\eta} M\left(\frac{a0+b0-4}{2}, 1+b0, \frac{-\Pr X}{\omega\alpha^2} e^{-\alpha\eta}\right) - c_2 e^{-2\alpha\eta} \tag{18}$$

where $c_1 = (1+c_2)/(M([a0+b0-4]/2, 1+b0, -\Pr X/\omega\alpha^2))$, $c_2 = Ec\Pr MnX^2 \operatorname{Sin}^2\gamma/[\omega\,\alpha^2(4-2a0)]$, and the parameters $a0$ and $b0$ are $a0 = \Pr X/\omega\alpha^2 = b0$. The non-dimensional wall temperature gradient obtained from (19) as:

$$\theta_\eta(0) = -c_1\alpha\left(\frac{ao+bo}{2}\right)M\left(\frac{a0+b0-4}{2}, 1+b0, \frac{-\Pr X}{\omega\alpha^2}\right) + c_1\left(\frac{ao+bo-4}{2(1-b0)}\right)\frac{\Pr X}{\omega\alpha} M\left(\frac{a0+b0-2}{2}, 2+b0, \frac{-\Pr X}{\omega\alpha^2}\right) + 2\alpha c_2 \tag{19}$$

The local heat flux can be written as

$$q_w = -\left(k + \left(\frac{16\sigma^* T_\infty^3}{k^*}\right)\right)(T_y)_{y=0} = -k\sqrt{\frac{a}{\vartheta}}(T_w - T_\infty)\left(\frac{3N+4}{3N}\right)\theta_\eta(0) \tag{20}$$

The local Nusselt number is defined as

$$Nu_x = \frac{q_w x}{k\left(T_w - T_\infty\right)}$$

3.2 Prescribed power law surface heat flux (PHF case)

The boundary conditions in PHF case are given by

$$\begin{aligned} -kT_y = q_w = A\left(\frac{x}{l}\right)^2 \quad \text{at} \quad y = 0 \\ T \to T_\infty \qquad \text{as} \qquad y \to \infty \end{aligned} \tag{21}$$

where A is constant, k and l are defined earlier. Define the non-dimensional temperature $g(\eta)$ as

$$g(\eta) = \frac{T - T_\infty}{T_w - T_\infty} \tag{22}$$

and make use of the transformation given by Eq. (4) and Eq. (22), leads to the following non-dimensional form of Eq.

(13) for temperature

$$\omega g_{\eta\eta} + \Pr f g_{\eta} - 2\Pr f_{\eta} g + Ec \Pr Mn f_{\eta}^2 \sin^2\gamma = 0 \tag{23}$$

The corresponding boundary conditions take the form

$$\begin{aligned} g_{\eta}(\eta) &= -1 \quad \text{at} \quad \eta = 0\,, \\ g(\eta) &\to 0 \quad \text{as} \quad \eta \to \infty \end{aligned} \tag{24}$$

An analytical solution of Eq. (23) subject to the boundary conditions in Eq. (24) is obtained in terms of confluent hypergeometric function as

$$g(\eta) = c_3 e^{-\alpha\left(\frac{a0+bo}{2}\right)\eta} M\left(\frac{a0+b0-4}{2}, 1+b0, \frac{-\Pr X}{\omega\alpha^2} e^{-\alpha\eta}\right) - c_2 e^{-2\alpha\eta} \tag{25}$$

where $a0$ and $b0$ and c_2 are as defined earlier in the PST case and c_3 is given below

$$c_3 = \frac{-1-2\alpha c_2}{-\alpha\left(\frac{ao+bo}{2}\right) M\left(\frac{a0+b0-4}{2}, 1+b0, \frac{-\Pr X}{\omega\alpha^2}\right) + \left(\frac{ao+bo-4}{2(1-b0)}\right)\frac{\Pr X}{\omega\alpha} M\left(\frac{a0+b0-2}{2}, 2+b0, \frac{-\Pr X}{\omega\alpha^2}\right)} \tag{26}$$

The non-dimensional wall temperature derived from (25) is read as:

$$g(0) = c_3 M\left(\frac{a0+b0-4}{2}, 1+b0, \frac{-\Pr X}{\omega\alpha^2}\right) - c_2 \tag{27}$$

4. Numerical Method for Solution

The non-linear differential equations (5) and (16) along with the boundary conditions (6) and (17) in PST case [(5) and (22) along with the boundary conditions (6) and (24) in PHF case] form a two-point boundary value problem and are solved using shooting iteration technique together with the fourth order Runge-Kutta integration scheme by converting it into an initial value problem. In this method we have to choose a suitable finite value of $\eta \to \infty$, say η_{∞}. We set following first order system:

$$\begin{aligned} q'_1 &= q_2 \\ q'_2 &= q_3 \\ q'_3 &= \left(\frac{\beta}{1+\beta}\right)\left(\left(q_2 + Mn\sin^2\gamma\right)q_2 - q_1 q_3\right) \\ q'_4 &= q_5 \\ q'_5 &= \frac{1}{\omega}\left(2\Pr q_2 q_4 - \Pr q_1 q_5 - Ec \Pr Mn\, q''_2 \sin^2\gamma\right) \end{aligned} \tag{28}$$

with the boundary conditions

$$\begin{aligned} &q_1(0) = 0, q_2(0) = 1 + Lq_3(0), \\ &q_4(0) = 1 \text{(For PST case)}, \\ &q_5(0) = \text{-}1 \text{ (For PHF case)}. \end{aligned} \tag{29}$$

To solve Eq. (28) with an initial value problem expressed by Eq. (29), we need the values for $q_3(0)$ i.e. $f_{\eta\eta}(0)$ and $q_5(0)$ i.e. $\theta_{\eta}(0)$ in PST case [$q_3(0)$ i.e. $f_{\eta\eta}(0)$ and $q_4(0)$ i.e. $g(0)$ in PHF case] but no such values are given. The initial guess values for $f_{\eta\eta}(0)$ and $\theta_{\eta}(0)$ [$f_{\eta\eta}(0)$ and $g(0)$ in PHF case] are chosen and the fourth order Runge-Kutta integration scheme is applied to obtain the solution. Then we compare the calculated values of $f_{\eta}(0)$ and $\theta(0)$ at $\eta \to \infty$ [$f_{\eta}(0)$ and $g(0)$ at $\eta \to \infty$ in PHF case] with the given boundary conditions $f_{\eta}(\eta_{\infty}) = 0$ and $\theta(\eta_{\infty}) = 0$ [$f_{\eta}(\eta_{\infty}) = 0$ and $g(\eta_{\infty}) = 0$ in PHF case] and adjust the values of $f_{\eta\eta}(0)$ and $\theta_{\eta}(0)$ [$f_{\eta\eta}(0)$ and $g(0)$ in PHF case] using shooting iteration technique to give better approximation for the solution. The process is repeated until we get the results correct up to the desired accuracy of 10–8 level, which fulfils the convergence criterion.

5. Results and Discussion

The solutions are obtained and plotted to discuss the effects of Ohmic dissipation and other relevant physical parameters on velocity profile, temperature profile, local skin friction coefficient, local Nusselt number and non-dimensional wall temperature. In these figures, blue line is low value, pink line is middle value and yellow line is the largest value of the physical parameters. The comparison is found to be in excellent agreement as shown in Table 1. We have compared the values of $\theta_\eta(0)$ and $g(0)$ with those of Turkyilmazoglu [25] for Newtonian fluid ($\beta \to \infty$) in the absence of aligned angle, velocity slip and radiation parameters.

5.1 Results for velocity profile

Fig. 1 shows the effect of magnetic parameter and angle parameter on the velocity profile. It is observed that the increasing values of magnetic parameter reduce the velocity boundary layer thickness. This is due to the fact that the increase in magnetic parameter increases the Lorentz force and it produces more resistance to the flow region. Effects of slip and porosity parameters on velocity profile are shown in Fig. 2. This is due to the fact that the increasing values of β lead to decrease yield stress which reduces the velocity profile and also due to the slip condition, the flow velocity near 11 the sheet is no longer equal to the stretching velocity of the sheet. The fluid velocity decreases because under the slip condition, the pulling of the stretching sheet can be only partly transmitted to the fluid and the velocity decreases with the slip parameter. It is clear from the figure that increasing values of slip and Casson parameters decrease the velocity boundary layer thickness.

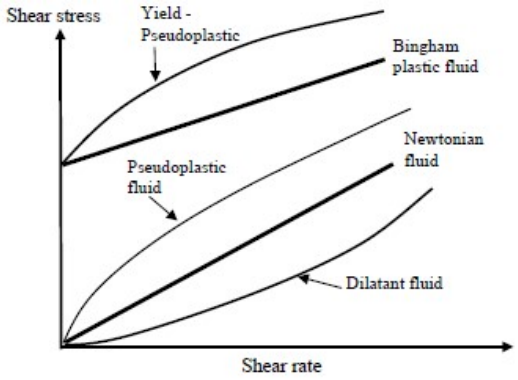

Fig. 1. Shear stress as a function of shear rate for several kind of fluid (Nguyen and Nguyen [27]).

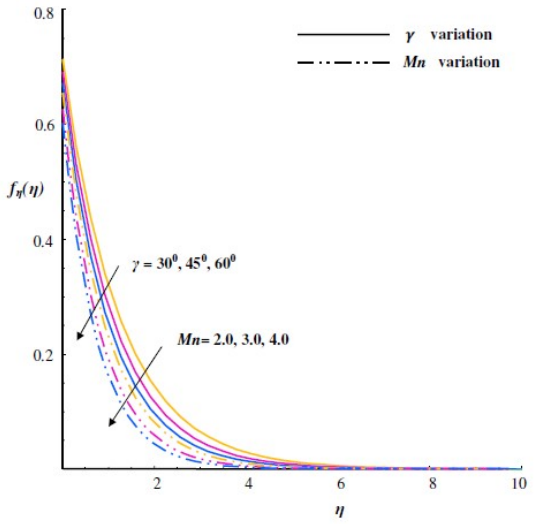

Fig. 2. Effect of magnetic and angle parameters on velocity profile with L = 0.5, β = 0.3, Mn=1 and γ=45^0.

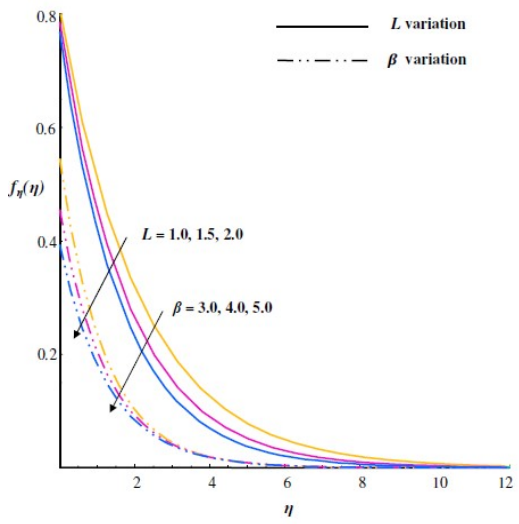

Fig. 3. Effect of slip and Casson parameters on velocity profile with L = 0.5, β = 0.3, Mn=1 and γ=45^0.

5.2 Results for temperature profile

The effects of magnetic parameter and angle parameter on the temperature profiles for both PST and PHF cases are presented in Figs. 3(a) and 3(b), respectively. Due to the enhancement in magnetic field strength, a resistive type force called Lorentz force associated with the aligned magnetic field makes the boundary layer thinner. Magnetic field lines of force move past the stretching sheet at the free stream velocity. The Casson fluid flow which is suppressed by the viscous action gets a push from the magnetic field which counteracts the viscous effects. The temperature profile increases with an increase in magnetic field for both prescribed surface temperature and power law surface heat flux cases. The

combined effect of magnetic and aligned angle parameter increases the thermal boundary layer thickness. Figs. 4(a) and 4(b) demonstrates the effect of Casson parameter and slip parameter on the temperature profile $\theta(\eta)$ in PST case and $g(\eta)$ in PHF case. The combined effects of Casson and slip parameters lead to increase the thickness of thermal boundary layer.

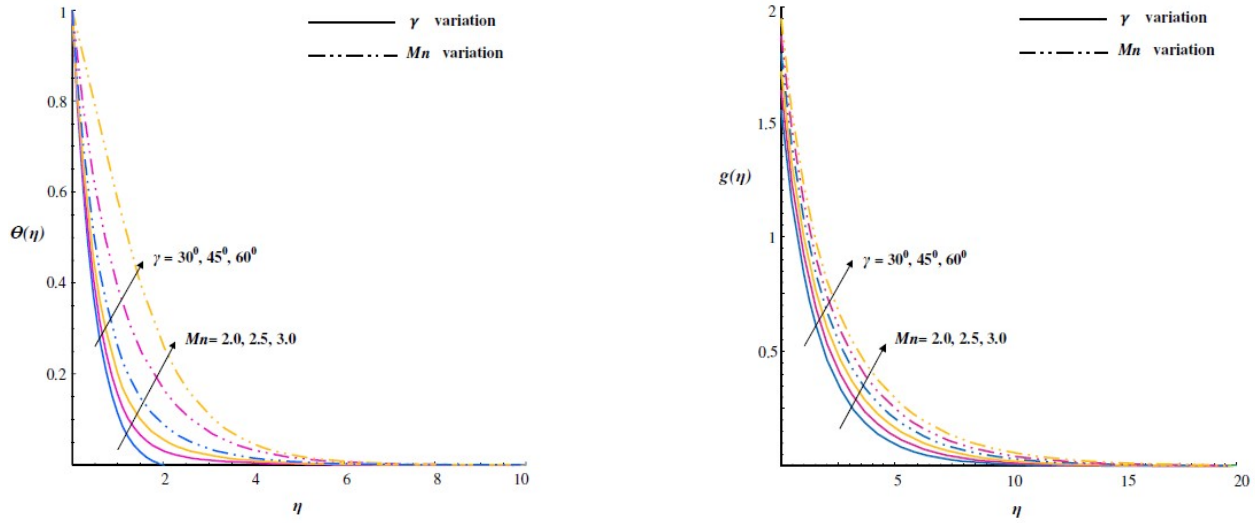

Fig. 4. Effect of magnetic and angle parameters on temperature profile (a) *θ(η) (PST case)* and (b) *g(η) (PHF case)* with L = 0.5, β = 0.3, N=1, Pr= 0.71, Mn=1, Ec=0.7 and γ=45^0.

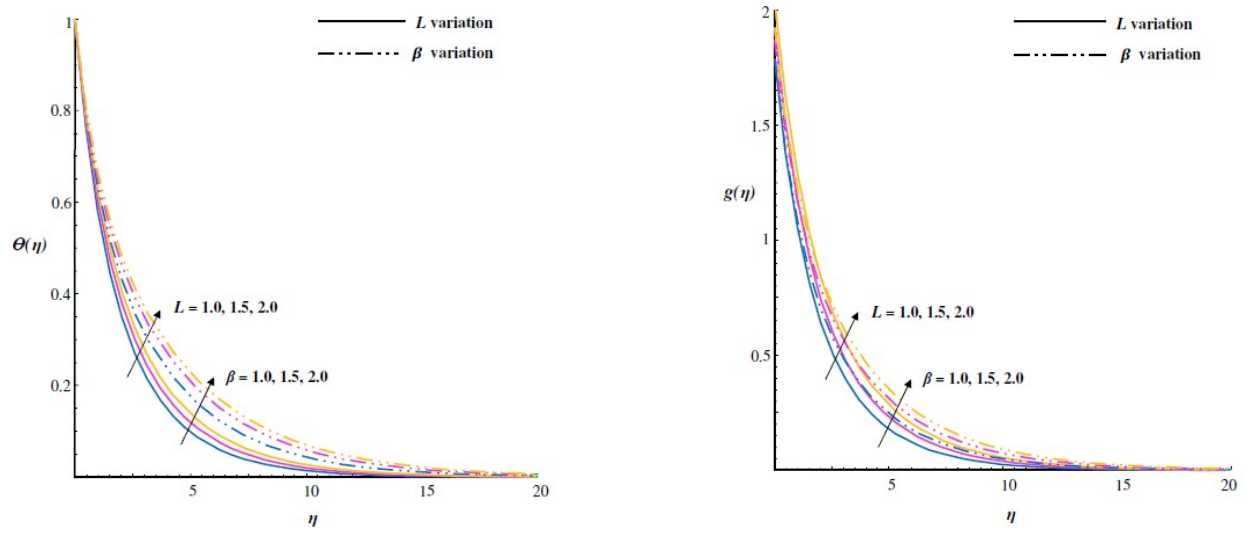

Fig. 5. Effect of slip and Casson parameters on temperature profile (a) *θ(η) (PST case)* and (b) *g(η) (PHF case)* with L = 0.5, β = 0.3, N=1, Pr= 0.71, Mn=1, Ec=0.7 and γ=45^0.

Figs. 5(a) and 5(b) depicts the effect of Prandtl number and radiation parameter on temperature profile for both PST and PHF case, respectively. Prandtl number is the ratio between momentum diffusivity to thermal diffusivity. In heat transfer problems, the Prandtl number controls thickness of the momentum and thermal boundary layers. When Prandtl number is small, heat diffuses quickly compared to the nanofluid velocity, which means that for liquid metals, the thickness of the thermal boundary layer is much bigger than the momentum boundary layer. Fluids with lower Prandtl number have higher thermal conductivities so that heat can diffuse from the sheet faster than for higher Pr fluids. The temperature profile decreases with the increasing values of radiation parameter in both PST and PHF case and same trend is observed on the Prandtl number. This is due to the fact that thermal boundary layer thickness decreases as radiation and Prandtl number increases.

Effects of Eckert number on the temperature profile are shown Fig. 6. It is noted that the increasing values of Eckert number increases the temperature profile. The Eckert number expresses the relationship between the kinetic energy in the flow and the enthalpy. It embodies the conversion of Kinetic energy into internal energy by work done against the viscous fluid stresses. Greater viscous dissipative heat causes a rise in the temperature profile. This is due to the fact that the heat energy is stored in liquid with the frictional heating.

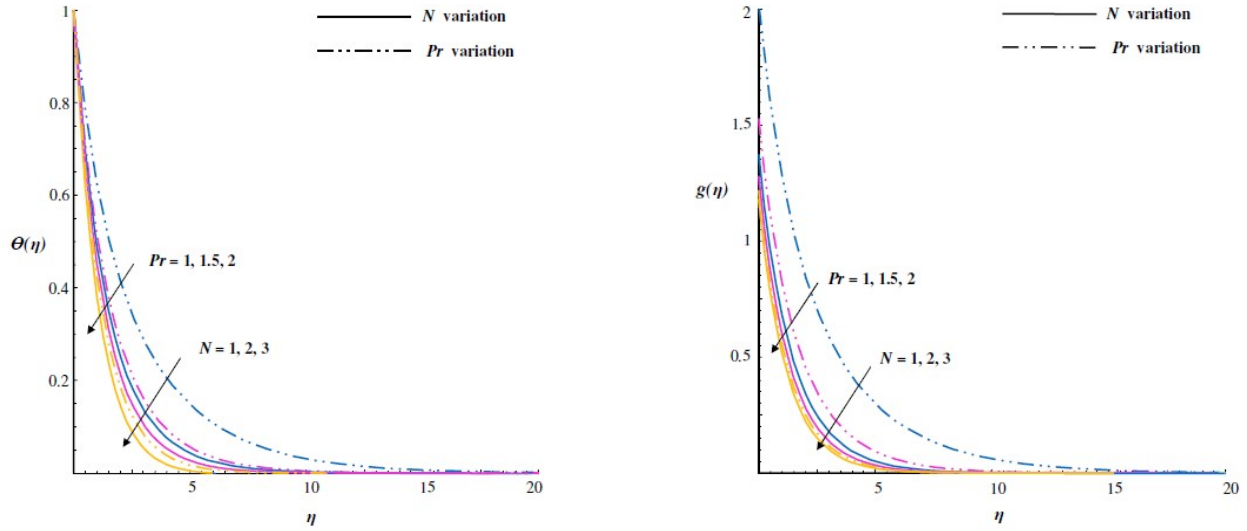

Fig. 6. Effect of Prandtl number and radiation parameter on temperature profile (a) *θ(η) (PST case*) and (b) *g(η) (PHF case*) with L = 0.5, β = 0.3, N=1, Pr= 0.71, Mn=1, Ec=0.7 and γ=45^0 .

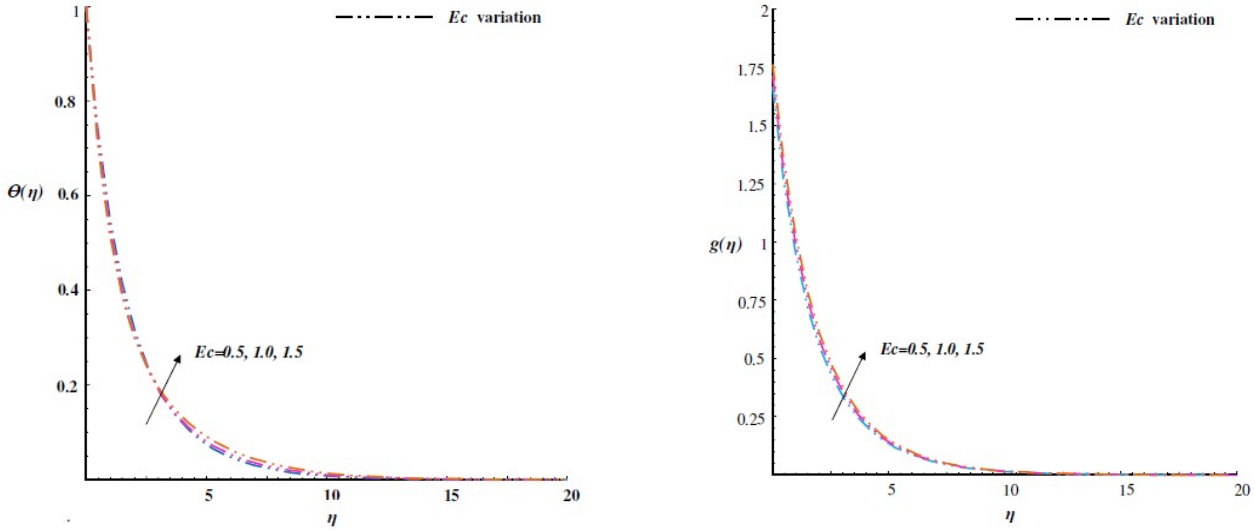

Fig. 7. Effect of Eckert number on temperature profile (a) *θ(η) (PST case*) and (b) *g(η) (PHF case*) with L = 0.5, β = 0.3, N=1, Pr= 0.71, Mn=1, Ec=0.7 and γ=45^0 .

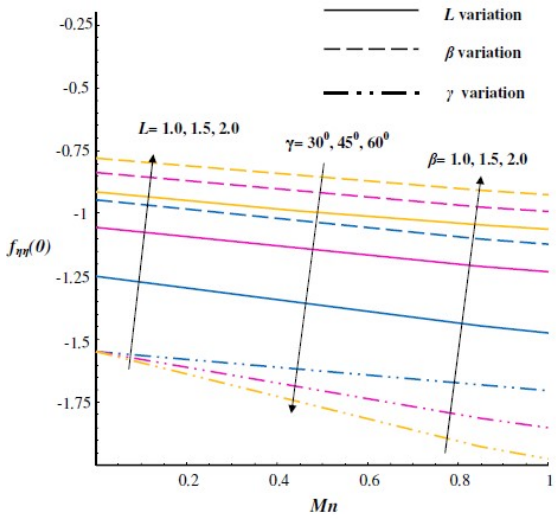

Fig. 8. Effect of magnetic, slip, angle and Casson parameters on local skin-friction $f_{\eta\eta}(0)$ with L = 0.5, β = 0.3, and γ=45^0 .

Table1. Comparison of $-\theta_\eta(0)$ and g(0) in PST and PHF cases

Mn	*Pr*	Turkyilmazoglu [25]		Present results			
				Analytical		Numerical	
		$-\theta_\eta(0)$	g(0)	$-\theta_\eta(0)$	g(0)	$-\theta_\eta(0)$	g(0)
0	1	1.3333	0.7500	1.3333	0.7500	1.33333	0.75000
	5	3.3164	--------	3.3164	0.3015	3.31648	0.30152
1	1	1.2157	0.82252	1.2157	0.8225	1.21577	0.82252
	5	---------	--------	3.2072	0.3117	3.20720	0.31179

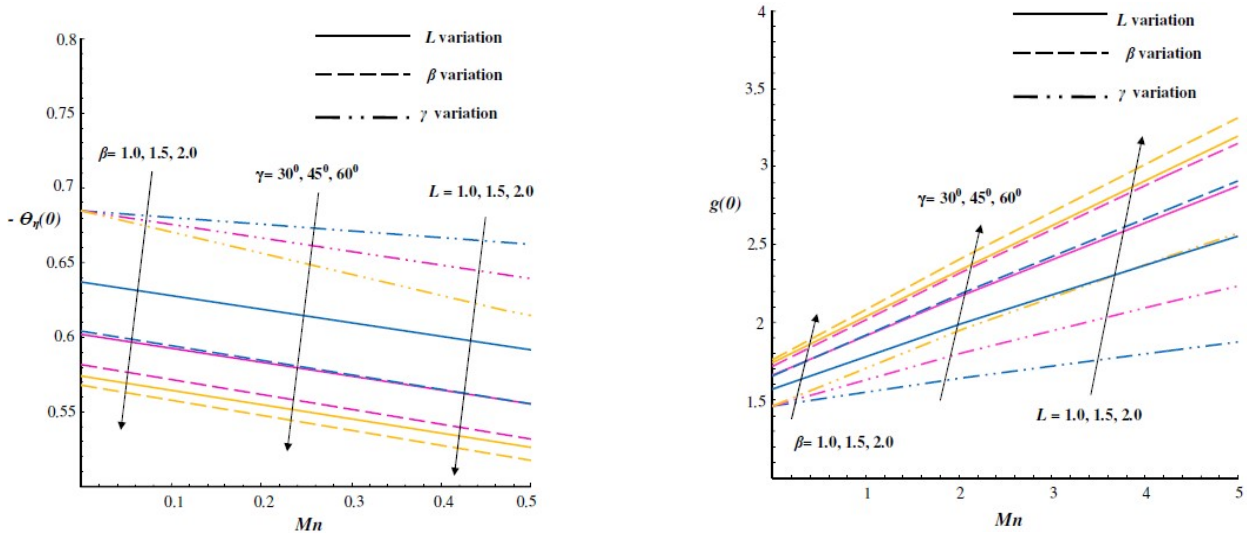

Fig. 9. Effect of magnetic, Slip, angle and Casson parameters on (a) local Nusselt number and (b) non-dimensional wall temperature with L = 0.5, β = 0.3, N=1, Pr= 0.71, Ec=0.7 and γ=450^0 .

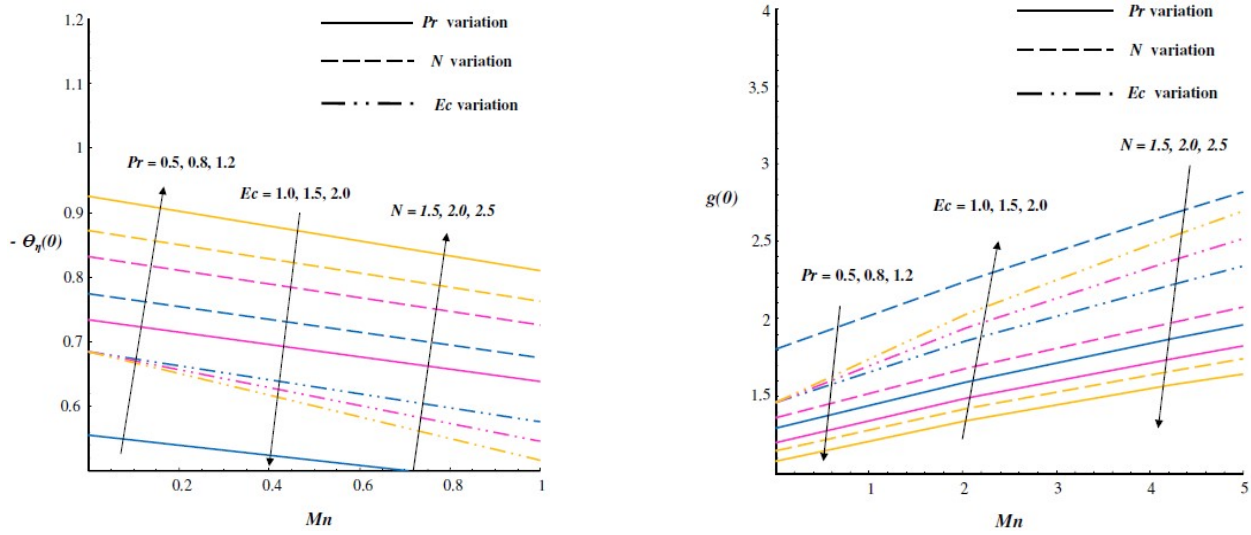

Fig. 10. Effect of Prandtl number, Eckert number and radiation parameter on (a) local Nusselt number and (b) non-dimensional wall temperature with L = 0.5, β = 0.3, N=1, Pr= 0.71, Ec=0.7 and γ=45^0.

5.3 Results for local skin friction coefficient

The combined effects of magnetic field with aligned angle, Casson parameter and the slip parameter on the local skin friction coefficient are display in Fig. 7. The magnetic parameter *Mn* is taken as *x*-axis and the local skin friction coefficient is taken as *y*-axis. It is clear that the local skin friction decreases with the increasing values of magnetic and angle parameters. The local skin friction coefficient enhances with the slip and Casson parameter and reduces with magnetic parameter.

5.4 Results for local Nusselt number and non-dimensional wall temperature

The combined effects of magnetic parameter with aligned angle, Casson parameter, slip parameter, radiation

parameter, Prandtl number and Eckert number on the local Nusselt number and non-dimensional wall temperature are demonstrated in Figs. 8-9 respectively. The local Nusselt number decreases with Mn and γ (Fig. 8(a)) and a reverse trend is observed on the non-dimensional wall temperature (Fig. 8(b)). The same trend is observed for β and L with magnetic parameter. It is noted that the increasing values of Prandtl number increase the local Nusselt number and decrease the non-dimensional wall temperature (Fig. 9(a) and 9(b)). Both local Nusselt number and non-dimensional wall temperature decreases with increasing N.

6. Conclusion

Ohmic dissipation effects of Casson fluid in the presence of inclined magnetic field over a stretching sheet with slip and thermal radiation is investigated. Using similarity transformation we converts the non-linear PDE to non-linear ODE. Both analytical and numerical solutions are obtained for governing momentum and energy equations and the following specific results are obtained.

- The velocity of the non-Newtonian fluid reduces with the increasing aligned angle of magnetic field, Casson parameter, velocity slip parameter and magnetic parameter.
- The effect of Eckert number is to increase the thermal boundary layer thickness. It also increases the non-dimensional wall temperature and decreases the local Nusselt number.
- An enhancement in the aligned angle of magnetic field decreases the local skin friction and local Nusselt number but increases the non-dimensional wall temperature.
- The aligned angle of the magnetic field plays an essential role in controlling the magnetic field power on the Casson fluid flow region.

Conflict of Interest

The authors declared no potential conflicts of interest with respect to the research, authorship and publication of this article.

Funding

The authors received no financial support for the research, authorship and publication of this article.

References

[1] D. Picchi , A. Ullmann , N. Brauner, Modelling of core-annular and plug flows of Newtonian/non-Newtonian shear-thinning fluids in pipes and capillary tubes, *Int. J. Multiphase Flow*, 103 (2018) 43-60.
[2] D. Picchi , P. Poesio , A. Ullmann , N. Brauner, Characteristics of stratified flows of Newtonian/non-Newtonian shear-thinning fluids, *Int. J. Multiphase Flow*, 97 (2017) 109-133.
[3]B. Mahanthesh, B.J. Gireesha, Thermal Marangoni convection in two-phase flow of dusty Casson fluid, *Res. Phys.*, 8 (2018) 537-544.
[4] S. V. Sailaja, B. Shanker, R. Raju, R. Srinivasa, Finite element analysis of magneto-hydrodynamic Casson fluid flow past a vertical plate with the impact of angle of inclination, *J. Nanofluids*, 7(2) (2018) 383-395.
[5] G. Kumaran, N. Sandeep, M.E. Ali, Computational analysis of magnetohydrodynamic Casson and Maxwell flows over a stretching sheet with cross diffusion, *Res. Phys.*, 7 (2017) 147-155.
[6] M. Hamid, M. Usman, Z.H. Khan, R. Ahmad, W. Wang, Dual solutions and stability analysis of flow and heat transfer of Casson fluid over a stretching sheet, *Phys. Lett. A*, https://doi.org/10.1016/j.physleta.2019.04.050.
[7] I. Ullah, S. Shafie, I. Khan, Effects of slip condition and Newtonian heating on MHD flow of Casson fluid over a nonlinearly stretching sheet saturated in a porous medium, *J. King Saud Univ. Sci.*, 29(2) (2017) 250-259.
[8] S.M. Ibrahim, G. Lorenzini, P. Vijaya Kumar, C.S.K. Raju, Influence of chemical reaction and heat source on dissipative MHD mixed convection flow of a Casson nanofluid over a nonlinear permeable stretching sheet, I*nt. J. Heat Mass Transfer*, 111 (2017) 346-355.
[9] G. Kumaran, N. Sandeep, Thermophoresis and Brownian moment effects on parabolic flow of MHD Casson and Williamson fluids with cross diffusion, *J. Mol. Liq.*, 233 (2017) 262-269.
[10] A.K. Abdul Hakeem, P. Renuka, N. Vishnu Ganesh, R. Kalaivanan, B. Ganga, Influence of inclined Lorentz forces on boundary layer flow of Casson fluid over an impermeable stretching sheet with heat transfer, J. *Magn. Magn. Mater.*, 401 (2016) 354-361.
[11] R. Kalaivanan, P. Renuka, N. Vishnu Ganesh, A.K. Abdul Hakeem, B. Ganga, S. Saranya, Effects of aligned magnetic field on slip flow of Casson fluid over a stretching sheet, *Procedia Eng.*, 127 (2015) 531-538.
[12] M.H. Abolbashari, N. Freidoonimehr, F. Nazari, M. M. Rashidi, Analytical modeling of entropy generation for Casson nano-fluid flow induced by a stretching surface, *Adv. Powder Technol.*, 26(2) (2015) 542-552.
[13] M.M. Rashidi, S. Bagheri, E. Momoniat, N. Freidoonimehr, Entropy analysis of convective MHD flow of third grade non-Newtonian fluid over a stretching sheet, *Ain Shams Eng. J.*, 8(1) (2017) 77-85.
[14] O.D. Makinde, W.A. Khan, J.R. Culham, MHD variable viscosity reacting flow over a convectively heated plate in a

porous medium with thermophoresis and radiative heat transfer, *Int. J. Heat Mass Transfe*r, 93 (2016) 595-604.
[15] M. Kayalvizhi, R. Kalaivanan, N. Vishnu Ganesh, B. Ganga, A.K. Abdul Hakeem, Velocity slip effects on heat and mass fluxes of MHD viscous-Ohmic dissipative flow over a stretching sheet with thermal radiation, *Ain Shams Eng. J.*, 7(2) (2016) 791-797.
[16] M. Sheikholeslami, D.D. Ganji, M. Younus Javed, R. Ellahi, Effect of thermal radiation on magnetohydrodynamics nanofluid flow and heat transfer by means of two phase model, *J. Magn. Magn. Mater.*, 374 (2015), 36-43.
[17] B. Ganga, S. Mohamed Yusuff Ansari, N. Vishnu Ganesh, A.K. Abdul Hakeem, MHD flow of Boungiorno model nanofluid over a vertical plate with internal heat generation/absorption, *Propul Power Res.*, 5(3) (2016) 211-222.
[18] B.J. Gireesha, B. Mahanthesh, I.S. Shivakumara, K.M. Eshwarappa, Melting heat transfer in boundary layer stagnation-point flow of nanofluid toward a stretching sheet with induced magnetic field, *Eng. Sci. Tech. Int. J.*, 19(1) (2016) 313-321.
[19] N. Sandeep, C. Sulochana, Dual solutions for unsteady mixed convection flow of MHD micropolar fluid over a stretching/shrinking sheet with non-uniform heat source/sink, *Eng. Sci. Tech. Int. J.*, 18(4) (2015) 738-745.
[20] D. Pal, G. Mandal, Thermal radiation and MHD effects on boundary layer flow of micropolar nanofluid past a stretching sheet with non-uniform heat source/sink, *Int. J. Mech. Sci.*, 126 (2017) 308-318.
[21] A.K. Abdul Hakeem, M.K. Nayak, O.D. Makinde, Effect of Exponentially Variable Viscosity and Permeability on Blasius Flow of Carreau Nano Fluid over an Electromagnetic Plate through a Porous Medium, *J. Appl. Comput. Mech.*, 5(2) (2019) 390-401.
[22] C.S.K. Raju, N. Sandeep, A. Malvandi, Free convective heat and mass transfer of MHD non-Newtonian nanofluids over a cone in the presence of non-uniform heat source/sink, *J. Mol. Liq.*, 221 (2016) 108-115.
[23] A.K. Abdul Hakeem, R. Kalaivanan, N. Vishnu Ganesh, B. Ganga, Effect of partial slip on hydromagnetic flow over a porous stretching sheet with non-uniform heat source/sink, thermal radiation and wall mass transfer, *Ain Shams Eng. J.*, 5 (2014), 913-922.
[24] C. Veeresh, M.C. Raju, S.V.K. Varma, A.G. Vijaya Kumar, Effects of Thermal Diffusion and Radiation on Magnetohydrodynamic (MHD) Chemically Reacting Fluid Flow Past a Vertical Plate in a Slip Flow Regime, *J. Appl. Comput. Mech.*, 5(2) (2019) 334-343.
[25] M. Turkyilmazoglu, Analytic heat and mass transfer of the mixed hydro-dynamic/ thermal slip MHD viscous flow over a stretching sheet, *Int. J. Mech. Sci.*, 53 (2011), 886-896.
[26] A. Mishra, A.K. Pandey, M. Kumar, Ohmic-viscous dissipation and slip effects on nanofluid flow over a stretching cylinder with suction/injection, *Nano Sci. Tech. Int. J.*, 9(2), (2018) 99–115.
[27] Q.H. Nguyen and N.D. Nguyen, *Incompressible non-Newtonian fluid flows*, Continuum Mechanics - Progress in Fundamentals and Engineering Applications, IntechOpen, DOI: 10.5772/26091, 47-72.

ORCID iD

R. Kalaivanan https://orcid.org/0000-0002-8303-4702